AIAA SciTech 2018
8 - 12 Jan 2018, Kissimmee, FL
AIAA-2018-0932

Modal Analysis of the Surface Pressure Field Around a Hemispherical Turret using Pressure Sensitive Paint

Nicholas De Lucca[1], Stanislav Gordeyev[2], Jacob Morrida[3], Eric J. Jumper[4]
University of Notre Dame, Notre Dame, IN, 46556

and

Donald J. Wittich[5]
Air Force Research Laboratory, Directed Energy Directorate, Kirtland AFB, NM 87117

Fast-response Pressure Sensitive Paint (PSP) measurements were performed on hemispherical models at transonic flow speeds. Both Proper Orthogonal Decomposition (POD) and Dynamic Mode Decomposition (DMD) were used to analyze the spatially and temporally resolved data. POD was used to isolate the dominant behavior in the data and isolate the dominant frequencies by looking at the temporal coefficient spectra. DMD was then used to further investigate specific frequencies. At St = 0.15-0.2, previously investigated "wake breathing" and "wake shifting" modes were found. These modes represent large spanwise symmetric and antisymmetric structures, respectively. Further, at St = 1 and St = 2, DMD showed that the wake of the turret was dominated by smaller convecting structures. The DMD modes were used to estimate the convective velocity in the wake, which was found to be relatively constant across various Strouhal Numbers.

I. Introduction

IT is desirable to have directed energy and free-space communications systems that can be operated on aircraft. For these systems, hemispherical turrets are often used to maximize field-of-regard. There has been extensive experimental work done to study these hemispherical turrets in the last decade. This work includes characterizing both the aerodynamic [1,2,3] and aero-optic [4,5,6] performance of the flow around the turrets at subsonic and transonic speeds. In addition to these experimental studies, there have been extensive CFD studies into the flow around hemispherical turrets [7,8,9,10,11].

At Mach numbers above 0.55, the flow over a hemisphere becomes locally supersonic, and an unsteady shock forms near the hemisphere surface close to the turret apex and the shock is found to oscillate within a few degrees of the apex [12]. Because of the large density gradients associated with the shock it causes an increased amount of optical distortions for side-looking angles. This problem could be overcome with adaptive optics; however, to correct for the shock-related aero-optical distortions, the instantaneous shock location and strength must be known. To predict these shock properties, the flow dynamics must be better understood. Optical and pressure measurements in both flight and tunnel tests indicate that there is a coupling between the shock and wake motion [13,14,15,16,17].

One way to study the shock-wake coupling is to analyze the spatio-temporal pressure field on the surface of and around the turret using fast-response Pressure Sensitive Paint (PSP). PSP measurements are based on oxygen-sensing molecules known as luminophore, which fluoresce when exposed to ultraviolet light [8,9]. Before the luminophore is added to the model surface, a permeable paint binder is applied, which allows oxygen diffusion. Oxygen quenches the luminescence of the paint, so as the air pressure increases, the oxygen concentration increases, which reduces the light emission. Therefore, the paint gets brighter as pressure decreases.

The pressure field on the surface of the turret has been extensively studied in the past and the experiment presented in this paper is a follow up on previous work using PSP [3,18]. The surface pressure field on the turret carries both the signature of the turbulent structures in the turret's vicinity and any global pressure modes over the turret. Both the global pressure modes and the turbulent structures have been shown to affect the optical performance of the turret

[1] Post-Doctoral Researcher, Department of Aerospace and Mech. Eng., Student AIAA Member
[2] Associate Professor, Department of Aerospace and Mech. Eng., AIAA Associate Fellow
[3] Graduate Research Assistant, Department of Aerospace and Mech. Eng., Student AIAA Member
[4] Professor, Department of Aerospace and Mech. Eng., AIAA Fellow
[5]Aerospace Engineer, Laser Division, 3550 Aberdeen Ave SE, AIAA Senior Member

[4,5,6]. Further, the unsteady loading on the turret is directly a function of the unsteady pressure field. The unsteady loading introduces undesired aero-mechanical beam jitter and might affect turret design. Thus, by understanding the pressure field over the turret, a better understanding of the flow features that are relevant to the optical performance can be attained and the design of optical turrets can be improved.

The goal of this paper is to examine the dominant flow features over a hemispherical turret through their surface pressure signature. To isolate the spatial and temporal characters of these modes, several types of modal decompositions will be used. Proper Orthogonal Decomposition (POD)[19,20,21] will be used to extract and study the most dominant spatial modes. POD naturally generates a set of basis vectors that maximizes the amount of energy per mode and thus is useful for locating where most of the "energy" in the flow is located. It is also useful for filtering out high spatial frequency modes [3], which are usually noisy. Dynamic Mode Decomposition (DMD) [22,23,24], on the other hand, decomposes the flow into a series of periodic modes at given frequencies. If the flow has dominant frequencies, it is useful to determine the dynamic character of the flow at these specific known frequencies. Both techniques will be used in a complimentary fashion in this paper. POD will be used to filter the data, determine the most energetic flow features and some of the dominant frequencies. DMD will then be used to further investigate flow topology and dynamics at those specific frequencies.

A companion paper [26] uses the same experimental data to study conditional wake response to different pressure fields on the hemisphere itself to better understand the wake dynamics at high subsonic and transonic speeds.

II. Experimental Setup

This experiment was performed in the Whitefield wind tunnel facility at the University of Notre Dame. This is a 3'x3'wind tunnel facility that is capable of up to M = 0.6 flow. A contraction was placed in the facility to increase the maximum freestream Mach number up to M = 0.7. Two different models were studied in this experiment, shown in Figure 1, diameter D = 10" hemisphere and D = 8" hemisphere. A schematic and picture of the setup are shown in Figure 2. A fast response, at least up to 10 kHz, Polymer-ceramic/PtTFPPF PSP formulation, manufactured by ISSI Inc., was used to measure the surface pressure field on the turret and in the wake behind the turret. To illuminate PSP, eight UV light sources, emitting in a narrow band about 400 nm, were placed on both sides of the test section. The UV lights were aligned with quartz inserts in the tunnel, Figure 2, to minimize absorption and reflection of the UV light. The PSP images were taken using three Phantom high speed cameras. The three cameras, Figure 2, used were a v1611 (Camera 1), a v1610 (Camera 2) and a v711 (Camera 3). Additionally, a set of 10 PSI differential Kulite sensors were placed both on the turret and at several locations in the wake to verify the PSP and perform an in-situ calibration.

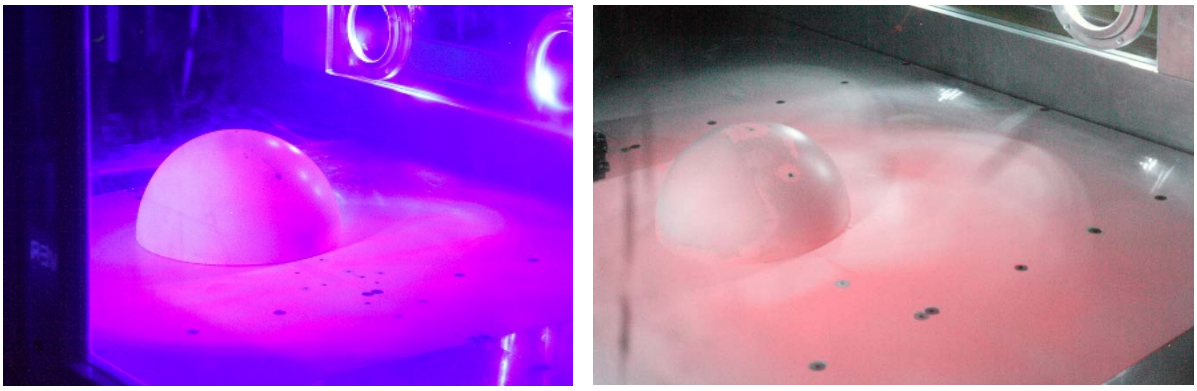

Figure 1: The tested turret geometries. Left is the 10" hemisphere. Right is the 8" hemisphere.

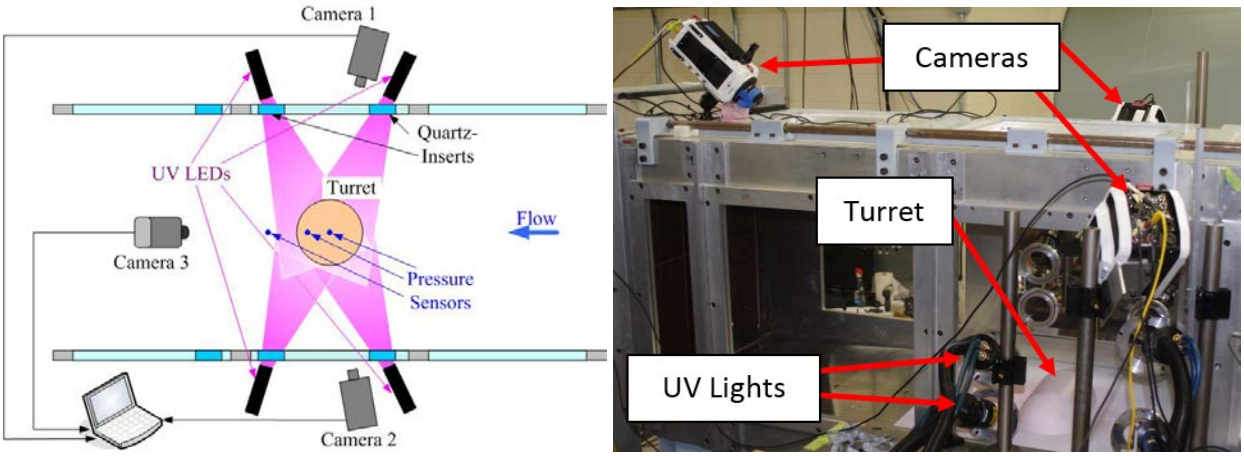

Figure 2: A schematic of the experimental setup, left and a picture, right.

The tunnel was run at various Mach numbers between M = 0.4 and M = 0.65. The maximum Mach number for each configuration varied slightly due to a different blockage by each model. Data were acquired at two different sample rates. The first sampling rate was 3 kHz for total of 32000 frames foe each camera. The second sampling rate was 10 kHz for total of 30000 frames for cameras 1 and 2. Because it was an older model with less sensitivity, for the second sampling tare, camera 3 was run at a lower sample rate of 2.5 kHz when the 10 kHz data was being acquired with the other two cameras. The Kulite data was acquired at 30 kHz. The three cameras were triggered simultaneously and the internal clocks were also synchronized. The Kulites were also triggered simultaneously with the cameras.

III. Data Analysis

Before analysis was done with the PSP videos, the Kulite pressure sensors were used to calibrate the paint. This was done by first extracting a small patch of intensity data, 10 pixel x 10 pixel, near a pressure port at the top of the hemisphere and spatially averaging to reduce noise, then comparing to the temporal pressure output from the Kulite.)The known linear relationship between the instantaneous intensity, I(t) and pressure, P(t), is given by

$$\frac{\overline{I(t)}}{I} = 1 + AP(t) \quad (1)$$

where the overbar indicates a mean, and P is the mean removed fluctuating pressure. The constant, *A*, was solved for by applying a linear fit to the instantaneous intensity ratio vs instantaneous mean removed pressure.

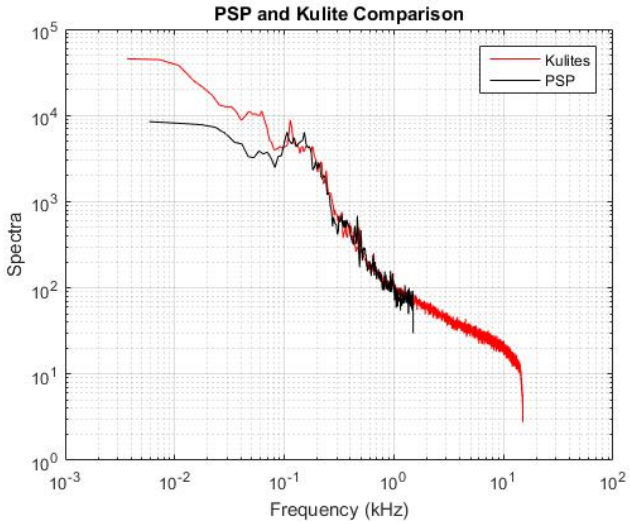

Figure 3: Power Spectra of the Pressure based on the Kulite (blue) and PSP (red) on top of the turret.

Using Eq. (1), the PSP luminescence intensity can be converted into pressure fluctuations. The images were pre-processed using a 10x10 Wiener filter. This filter is efficient at removing shot noise from the camera images. The

paint was found to correctly resolve the unsteady pressure spectrum up to a frequency around 500 Hz, see Figure 3. Above it, pressure fluctuations were smaller than PSP sensitivity, resulting in a flat noise-dominated part of the spectrum.

Both Proper Orthogonal Decomposition (POD) and Dynamic Mode Decomposition (DMD) were used to analyze the data at different Mach numbers. To compute POD modes and corresponding temporal coefficients, a widely-accepted algorithm using a Singular Value Decomposition (SVD) was used [23].

The algorithm used for DMD is outlined in [22,23,24,25]. DMD decomposes the pressure field, P, into spatial modes, φ, eigenvalues, λ, to represent the frequency and exponential decay rate of the modes and amplitudes, c,

$$P\left(\vec{x},t\right)\approx\sum_{k=1}^{n}c_k e^{\lambda_k t}\phi_k\left(\vec{x}\right). \tag{2}$$

Note that the modes, φ, and the amplitudes, c, are complex quantities. This is done by breaking the pressure data set into two data sets, P_1 and P_2. If the data set has N total frames of pressure from PSP, P_1 contains the first $N-1$ frames and P_2 contains the last $N-1$ frames given by

$$\begin{aligned} P_1 &= \{p_1, p_2, \ldots, p_{N-1}\} \\ P_2 &= \{p_2, p_3, \ldots, p_N\} \end{aligned}; \tag{3}$$

essentially the two data sets are offset by a single time step. The goal is to find a matrix A such that the second data set is written as a linear combination of the first data set,

$$P_2 = AP_1. \tag{4}$$

This matrix is called the companion matrix. An estimate to it, S is determined by

$$P_2 = AP_1 = P_1S - r,\ S = \arg\min\left\|P_2 - P_1S\right\| \tag{5}$$

where r is the residual. A and S are similar in that they share the same eigenvalues. The eigenvectors between the two matrices are related as well.

The actual computation of the DMD modes starts with SVD of the first data set, P_1:

$$P_1 = U\Sigma W^H, \tag{6}$$

where the H superscript denotes the Hermitian transpose. The above relationship between P_1, P_2 and S, can have the SVD of the first data set substituted in,

$$\begin{aligned} P_2 &= U\Sigma W^H S \ \text{ and} \\ S &= UP_2\Sigma^{-1}W = U^H AU = Y\mu Y^{-1}. \end{aligned} \tag{7}$$

Here μ and Y are the eigenvalues and eigenvectors of the eigenvalue problem of S,

$$SY = \mu Y. \tag{8}$$

The DMD modes and eigenvalues can be computed from the eigenvectors and eigenvalues of S by

$$\phi = P_2Y,\ \lambda = \ln(\mu)/\Delta t. \tag{9}$$

The frequency and exponential decay rate of the DMD modes can be found in the eigenvalues. The frequency is given by the imaginary part of the eigenvalue and the decay rate is given by the real part,

$$e^{\lambda_k t} = e^{\mathrm{Re}(\lambda_k)t + i\,\mathrm{Im}(\lambda_k)t}. \tag{10}$$

To find the expression for c_k-coefficients in Eq. (2), we can substitute the decomposition of S into the relationship between V_1 and V_2 above,

$$P_2 = P_1S = P_1Y\mu Y^{-1} = \phi\mu Y^{-1} = \phi c_k, \tag{11}$$

Here μY^{-1} serves the same role as the temporal coefficients, c_k, of standard POD decomposition,

$$P_2 = \sum_{k=1}^{N-1}\phi_k c_k(t). \tag{11}$$

IV. Results

A. POD Results

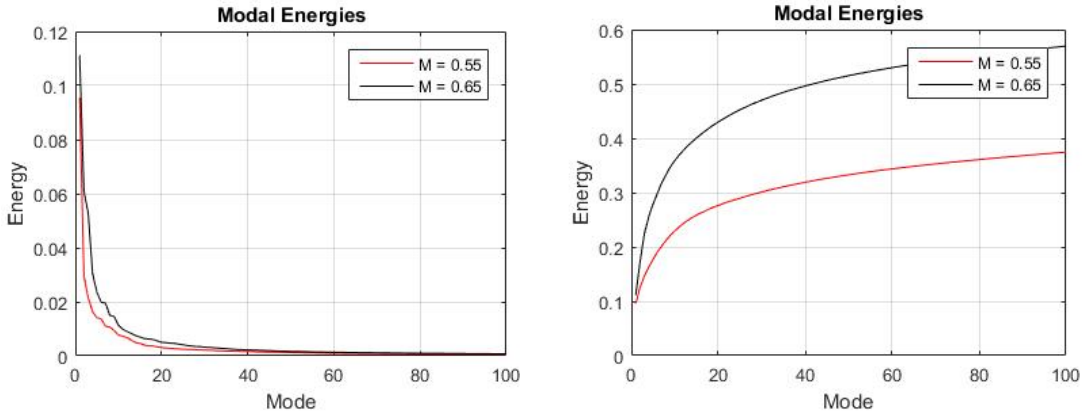

Figure 4: The POD energy distribution, left, and cumulative energy distribution, right, for M = 0.65 and M = 0.55.

The POD modal energy distributions are shown in Figure 4. The modes themselves are shown in Figure 5 for M = 0.55 and Figure 6 for M = 0.65. While the cumulative energy distributions, Figure 4, right, look very different between M = 0.65 and M = 0.55, the energy per mode, shown in Figure 4, left, shows that the difference is mostly that each of the M = 0.65 modes have slightly higher energy in each mode. This means that the that the flow is more ordered across all the modes at M = 0.65. The first two modes are "wake shifting" modes at both M = 0.55 and M = 0.65. This "wake shifting" has an anti-symmetric character on the turret itself, as schematically shown in Figure 7, and was observed in prior PSP experiments [3, 27]. The "wake shifting" is likely caused by very large structures shed off alternating sides of the turret [27]. This represents as a movement of the separation line on the turret itself. In the wake, this is visible in the first POD mode for both Mach numbers, see Figures 5 and 6, as alternating phase pressure fluctuations moving downstream from the turret sides. At M = 0.65, the "wake shifting" mode correlates with shock movement along the turret sides. The shock induces separation on the turret side, so it's expected to correlate with this bulk motion of the turret wake. The first wake shifting mode is stronger at M = 0.55 than M = 0.65. This is likely due to the second mode being corrupted by camera noise, present as stripes for negative y-locations, see Figure 5, top right.

At M = 0.55, modes 3 and 4 represent a "wake breathing" phenomenon [27], schematically shown in Figure 8. These two modes are spatially out of phase and contain large wake structures, which combine to form spanwise-symmetric convecting structures in the wake. These modes are characterized by large structures off the turret apex and in the centerline of the wake. The "wake breathing" comes from the wake expanding outward in the wall normal direction while shrinking along the sides. On the turret, it represents as pressure fluctuations along the turret sides that are in-phase and pressure fluctuations along the downstream centerline that are out of phase with the turret sides [3]. In the wake, this "wake breathing" represents as large-scale structures in the wake with alternating phase along the downstream direction. At M = 0.65, the "wake breathing" mode also correlates with upstream and downstream motion of the shock over the top of the turret. Modes 3 and 4 at M = 0.55 represent convecting structures in the wake. Mode 4 is also correlated, although weakly, with the necklace vortex, located just upstream of the turret.

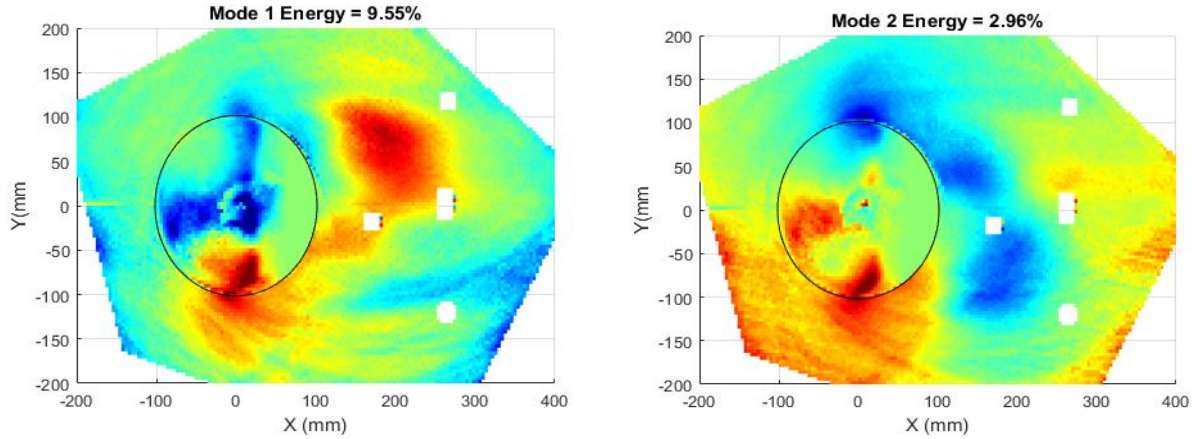

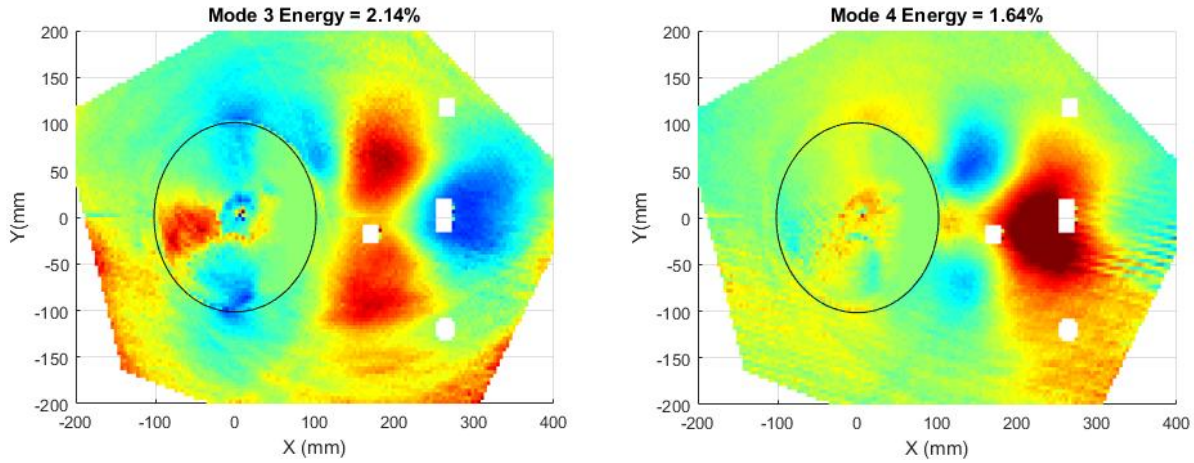

Figure 5: The first four POD modes for M = 0.55.

The temporal coefficient spectra for different normalize frequencies, St = fD/U_∞, for the first four modes at M = 0.55 and M = 0.65 are shown in Figure 9. The "wake shifting" mode at M = 0.55 has a peak around St = 0.15. This is close to the St = 0.15 peak that was observed for the first POD mode on a full hemisphere-on-cylinder turret [3, 27]. The peak is closer to St = 0.19 at M = 0.65. The "wake breathing" mode for both Mach numbers has more energy in the lower frequencies than the "wake shifting" mode for both Mach numbers. It has a peak at St = 0.13-0.15 for both Mach numbers as well. For modes 3 and 4 at M = 0.55 and mode 4 at M = 0.65, there is an increase in modal energy between St = 0.2 and St = 0.7. This increase corresponds to the smaller structure size seen in these modes compared to the first 2-3 modes, respectively. Knowing the dominant frequencies for these modes, DMD will be applied in the next section to investigate them further.

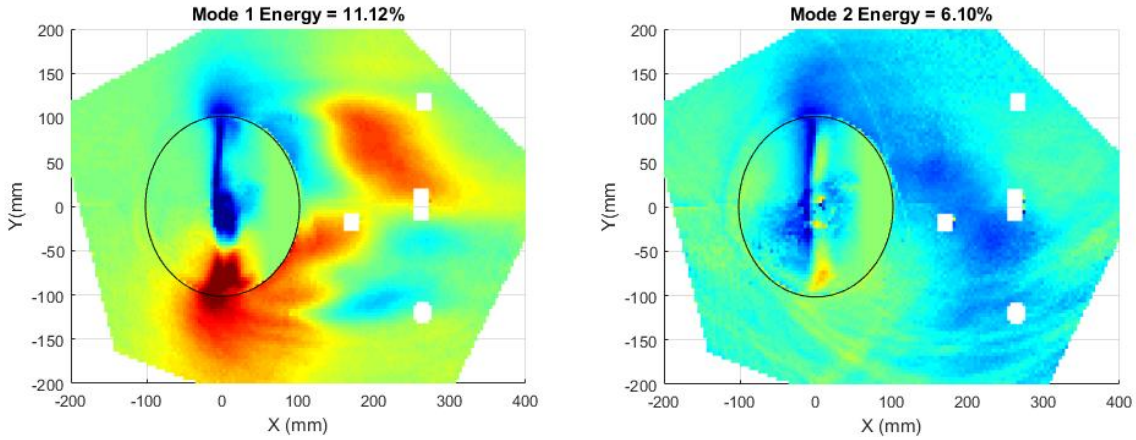

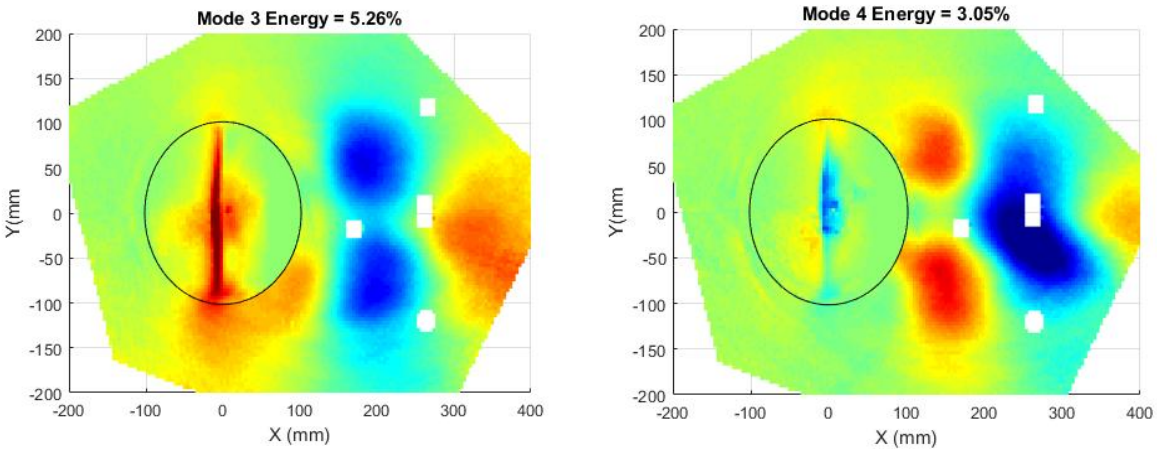

Figure 6: The first four POD modes for M = 0.65.

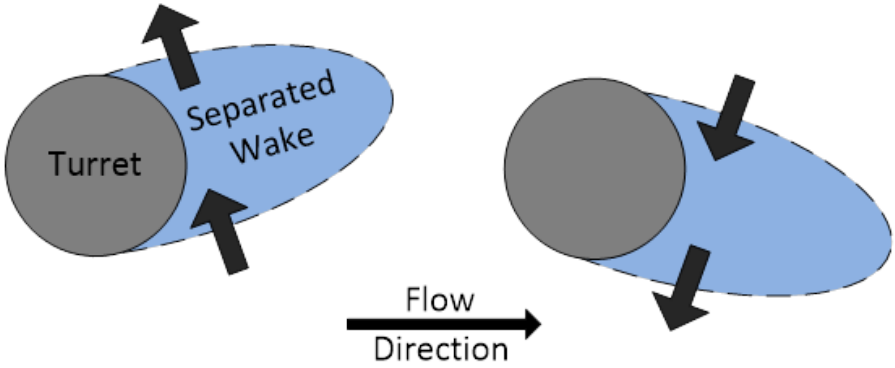

Figure 7: A schematic of the wake "shifting" mode.

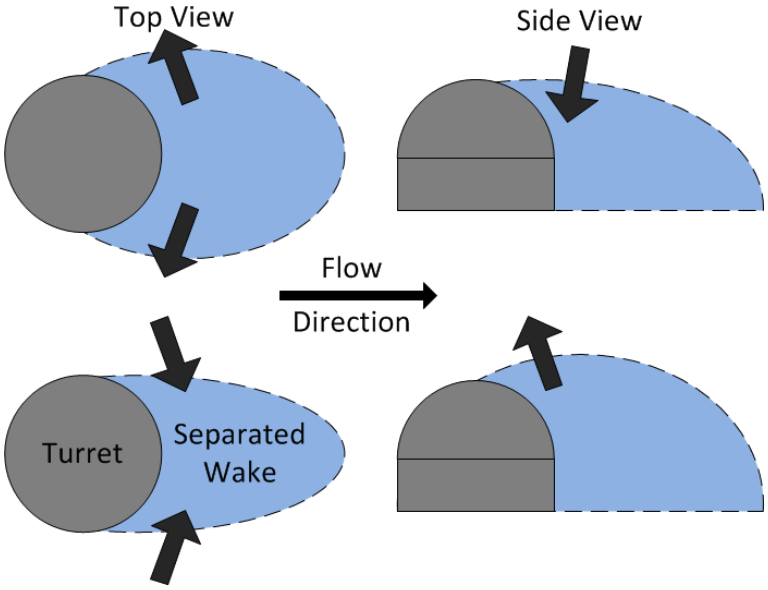

Figure 8: A schematic of the wake "breathing" mode.

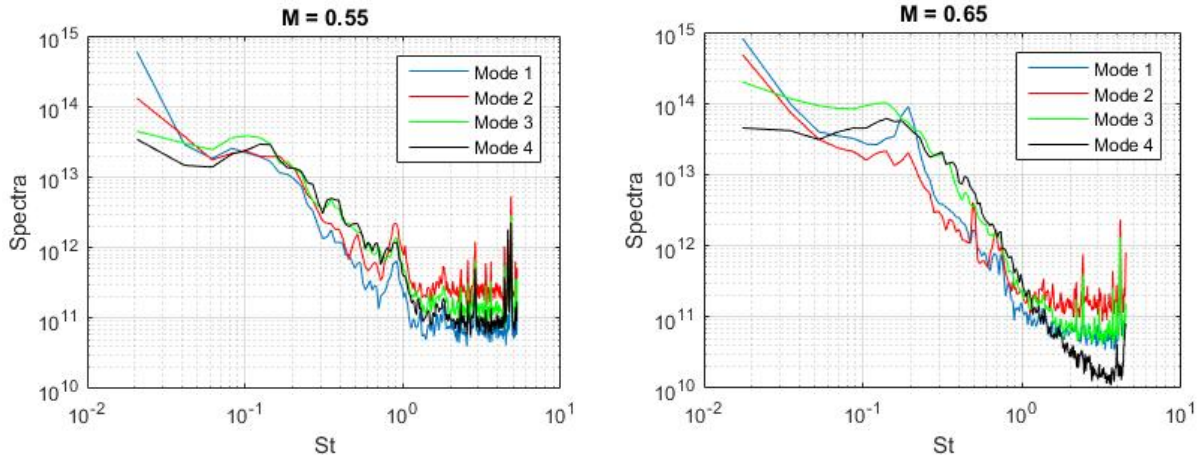

Figure 9: The temporal coefficient spectra for M = 0.55, left and M = 0.65, right.

The higher order modes for M = 0.65 are shown in Figure 10. These modes all represent increasingly smaller scale structures in the wake. Each pair of these modes represent convecting structures in the turret wake. Each mode has a spatially out-of-phase pair that allows the combination of the two to represent a convective structure. These structures also correlate with the motion of the shock. Again, this is expected, as the shock induces separation and thus should correlate with the structures shed off the turret. These modes also correlate slightly with the necklace vortex located upstream of the turret. The modal spectra, shown in Figure 11, show similar trends as those for the first 4 modes. All the modes capture finer motion of the shock and have peak at St = 0.18-0.2. They all have increased higher frequency content that corresponds to the smaller structure size relative to the first 4 modes. The spectral tail shows more aliasing as the mode number increases, further evidence of increasing higher frequency spectral content. Though not shown, even higher order modes represent smaller and smaller convecting structures in the wake. Because the first 8 modes predominantly feature wake structures and the signature of the "wake shifting" and "wake breathing" effects on the turret, the wake modes are the most energetic feature of the surface pressure field around and just downstream of the turret.

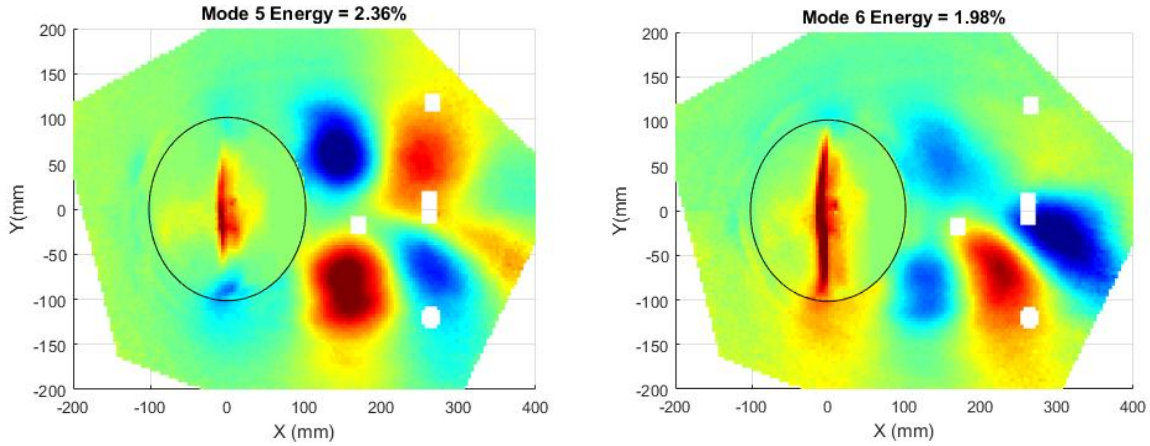

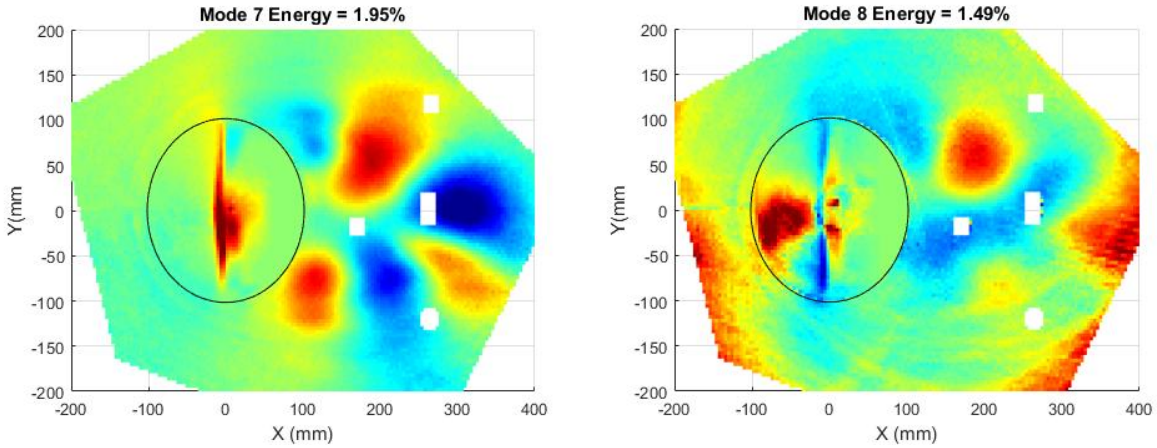

Figure 10: Higher order POD modes for M = 0.65.

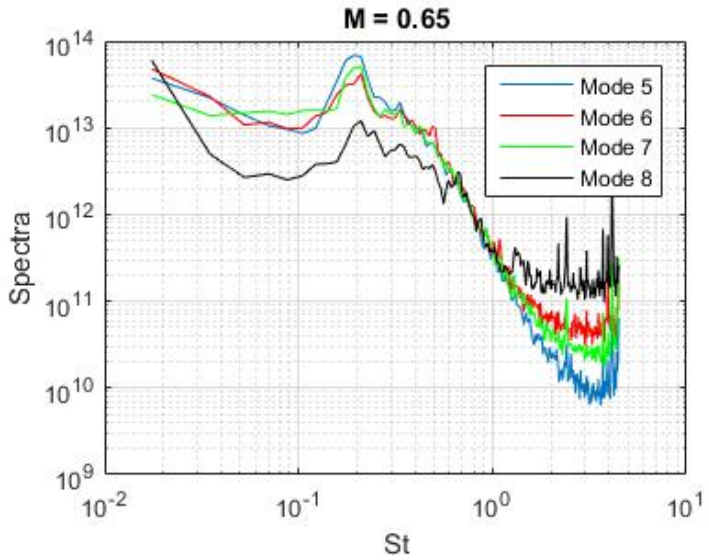

Figure 11: The temporal coefficient spectra for modes 5-8 at M = 0.65.

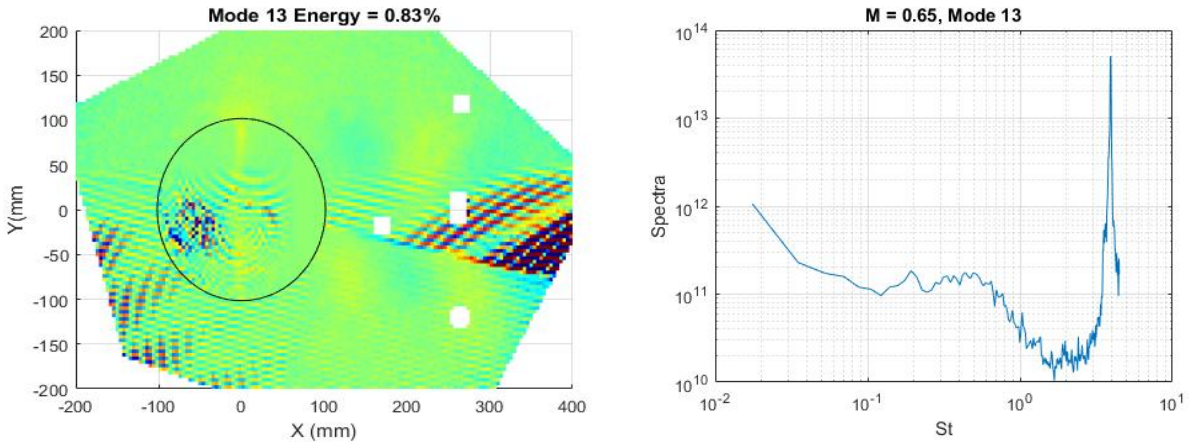

Figure 12: Sample POD mode at M = 0.65 that contains camera noise, left and its spectra, right.

To demonstrate the effectiveness of POD technique to identify various noise sources in the data, Figure 12 shows the modal shape and spectra for mode 13, at M = 0.65. This mode contains very high spatial frequency variations in

only one half of the flow field, for negative y-locations. This variation is likely due to camera noise, as flow features are highly unlikely to be this ordered or regular; also, these features are not present for positive y-locations. The spectrum of this mode shows a very sharp peak at St = 3.9, corresponding to f = 4415 Hz. In additional to these ordered spatial features, mode 13 also includes some of the physical flow features. This shows one of the limitations of the POD technique: noise can be coupled into relevant modes and inhibit analysis of the data. As will be shown in the next section, DMD can be useful to isolate single-frequency noise.

Overall, POD is a useful technique for isolating the dominant features in a set of a data. In this case, it shows the most energetic surface pressure modes of the flow field over the turret. By investigating the spectral content of the POD temporal coefficients, dominant frequencies can be determined for these most energetic features as well. Because the modes are orthogonal, it might be useful for constructing a low order model of the flow features. However, POD isn't necessarily useful for removing just noise content. The noise can be coupled with physically-relevant modes and interfere with the analysis or low-order reconstruction. POD works well as a companion technique to DMD in that it can show what is most important in the flow and give the relevant frequencies to investigate using DMD.

B. DMD Results

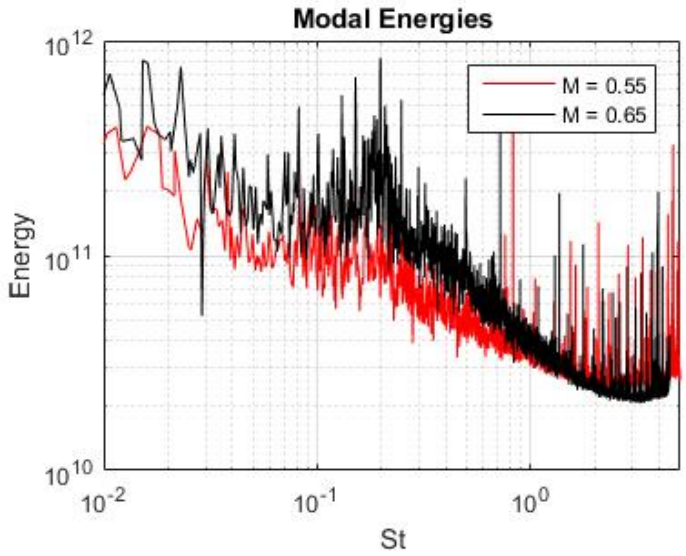

Figure 13: DMD modal energies as a function of Strouhal number for M = 0.65 and M = 0.55 for an 8" turret.

Figure 13 shows the energies of the DMD modes, $|c_k|^2$, from Eq. (2). The modal amplitudes give an energy spectrum for the pressure fluctuations as a function of frequency. There are a couple important frequency regions to investigate using the DMD. First, the separation line movement on the turret and the shock motion have been shown to have a spectral peak around the $St = fD/U_\infty$ = 0.15-0.3 range [3,6]. Second, smaller turbulent structures near the turret base have been observed near St = 1 [27]. This higher frequency range was also associated with the most optically-aberrating structures in the turret wake [13]. Applying DMD technique, we also observed a local increase in the DMD modal energies at St = 0.15-0.2, which is close to the expected motion of the separation line and the shock movement peak at St = 0.15, see Figure 13. This is the same frequency range that the wake "shifting" and "breathing" modes were observed in the POD analysis. Comparing DMD spectra both Mach numbers, the lower frequency modes, St < 1.5, are more energetic at M = 0.65 than M = 0.55. This is due to the fact that pressure fluctuations overall are larger at M = 0.65 due to the higher speed.

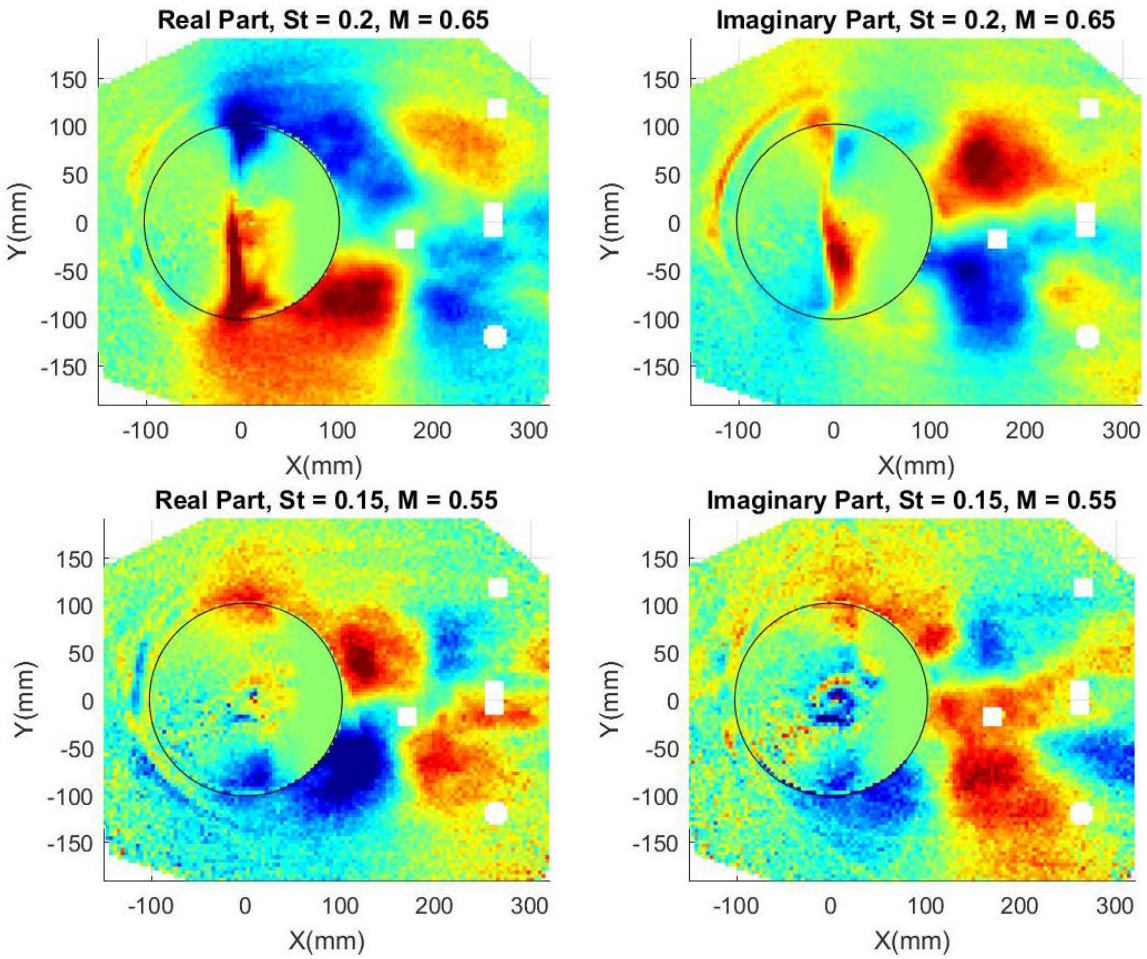

Figure 14: The mode shapes at St = 0.2 for M = 0.65 (Top) and St = 0.135 at M = 0.55 (Bottom) with an 8" turret.

The DMD modes, both real and imaginary parts, near St = 0.15-0.2 for M = 0.55 and 0.65 are shown in Figure 14. At M = 0.65, Figure 14, top, the real and imaginary parts of the modes feature strong mostly spanwise-uniform structures across the entire wake. It implies that at this frequency, these large wake structures are strongly correlated with the shock over the top of the turret. Examination of the DMD structure on top of the turret revealed a predominantly upstream motion of the shock; this dynamic behavior was observed and optically studied in [5] at similar transonic speeds. In contrast, at M = 0.55, Figure 14, bottom, the shock is absent on the turret. The large structures in the wake at this Mach number, appear to be less-spanwise organized, but still occupy the entire wake region. This indicates that the wake motion is of a global, large-scale nature. Also, this indicated that the shock at transonic speeds is correlated with the global wake motion on the hemisphere at this frequency and the presence of the shock forces the structures in the wake to be more organized.

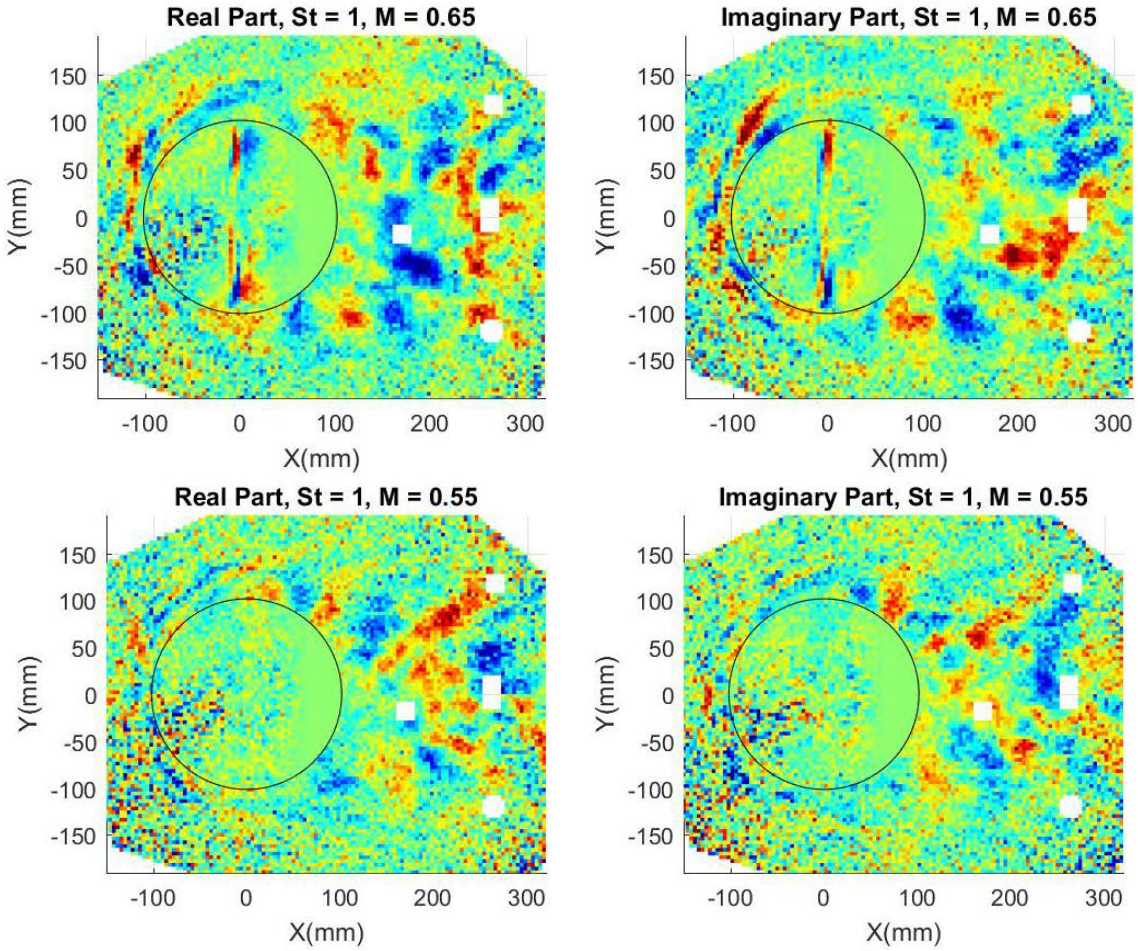

Figure 15: The mode shapes at St = 1 for M = 0.65 (Top) and M = 0.55 (Bottom) with an 8" turret.

The DMD pressure mode for St = 1 at M = 0.65 is shown in Figure 15, top. In [3, 27] this Strouhal number was associated with small turbulent convecting structures being shed off the turret into the wake. Similar small-scale convecting features are present in the DMD mode at M = 0.65 on the hemispherical turret. Unlike the large-scale structures for St = 0.15, shown in Figure 14, these structures are primarily present in the separated shear-like region along the boundary of the separation region, as well as in the center of the wake region. Interestingly, the necklace vortex in front of the hemisphere also exhibits movement at this Strouhal number, as evidenced by the varying phase of the pressure fluctuations just upstream of the turret. Notably at M = 0.65, there are small local movements of the shock at these frequencies too. For M = 0.55, Figure 15, bottom, very similar structures are observed in the wake. These structures appear to be more organized, compared to M = 0.65, and primarily reside in the separation interface. There is also some necklace vortex movement at this Mach number as well, however, there isn't much evidence of any separation line movement being tied to these structures in the modes.

The DMD pressure modes at St = 2 for M = 0.65 and M = 0.55, Figure 16, top and bottom respectively, display similar behaviors to those at St = 1. At this frequency, the convecting structures are located primarily in the shear-dominated region between the downstream-moving flow and the recirculation region immediately downstream of the hemisphere. This suggests that these surface pressure structures are related to the vortical shear-layer structures, formed when the flow separates off the turret. It is consistent with the findings that aero-optical distortions in the wake, thought to be primarily due to shear-layer structures, are dominant at this Strouhal number [13]. Additionally, at this Strouhal number, there are no shock-related motions present. Assuming that these small structures are inside the interface region between the upcoming flow and the recirculating region downstream of the hemisphere, the recirculation region appears to be smaller for M = 0.55, see Figure 16, bottom, than for M = 0.65, see Figure 16, top; similar conclusions were made using the oil-based surface flow visualization studies around the hemisphere [15]. The higher order modes also show a weakness of DMD: local shot noise begins to corrupt the modes. POD, on the other hand, pushes this higher frequency, uncorrelated noise to the highest order modes.

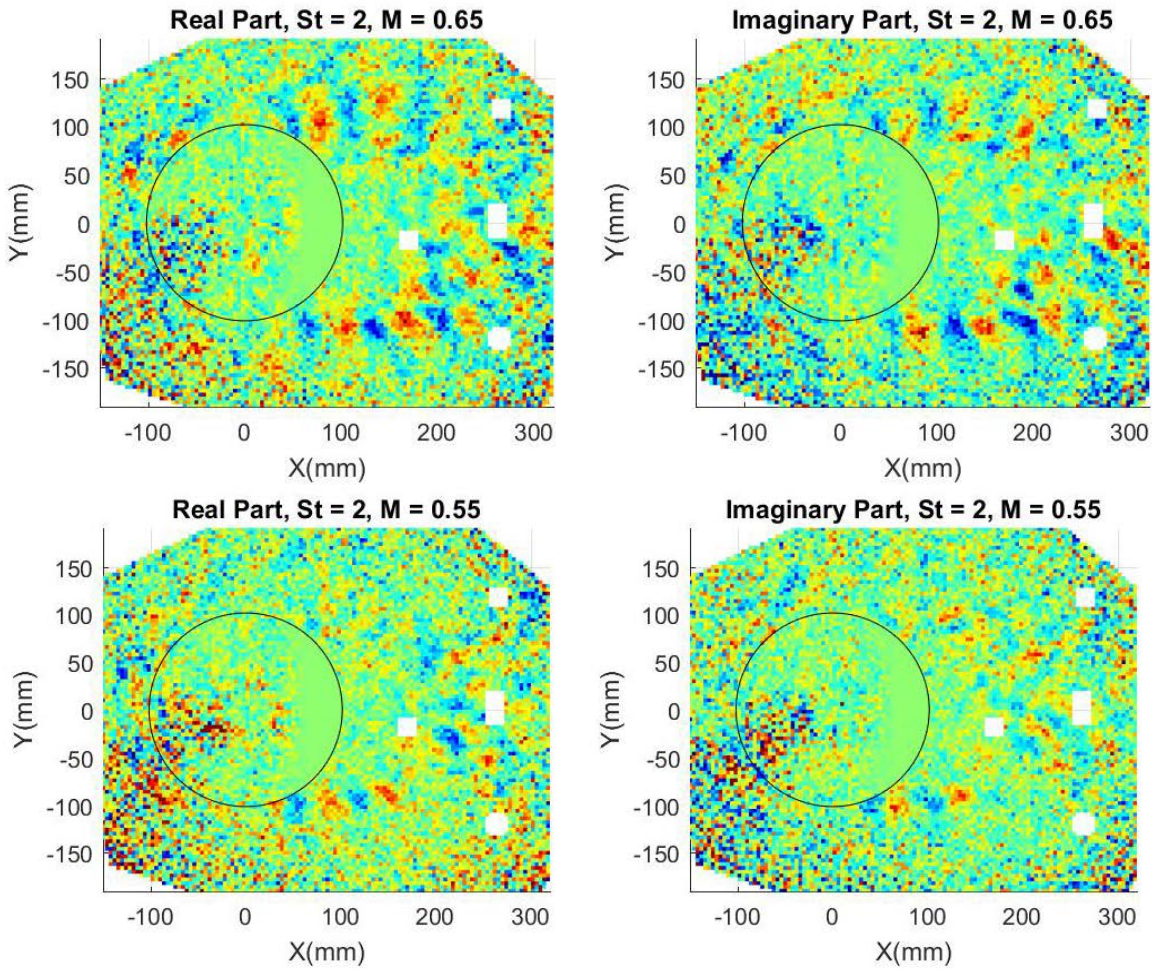

Figure 16: The mode shapes at St = 2 for M = 0.65 (Top) and M = 0.55 (Bottom) with an 8" turret.

DMD can be used to isolate the single frequency camera-noise-related observed previously using the POD. By looking at the mode closest to the f = 43415 Hz peak seen previously in Figure 12, right, the camera noise can be better isolated. This single mode, presented in Figure 17, shows a very similar character to the POD mode, shown in Figure 12, but the structure size of the flow structures is much smaller in the DMD mode compared the POD mode. That is because the DMD mode structures as sized based on the frequency, not the energy content. If a reconstruction was performed using the DMD modes, eliminating this single mode would be equivalent to notch filtering the data at this frequency. Because of the smaller structure size, less energy would be removed from the actual flow reconstruction than if filtering would be done using POD.

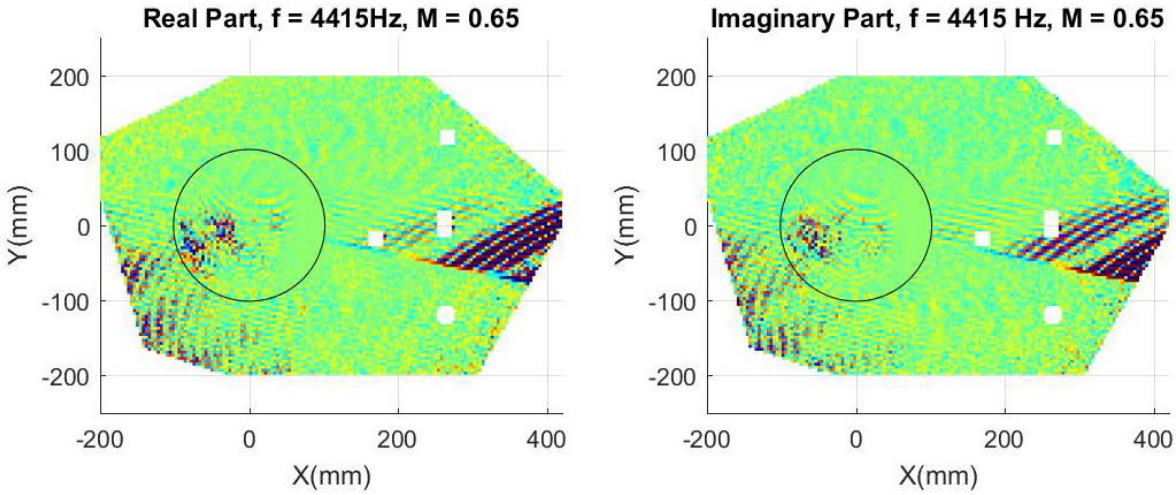

Figure 17: DMD Mode that contain noise from digital camera.

Convective Speed Estimates

As each DMD mode corresponds to the time-periodic pressure field,

$$P = e^{\lambda_k t}\phi_k\left(\vec{x}\right) = e^{\varphi}\phi_k\left(\vec{x}\right),$$

the DMD modes can also be used to estimate the convective speed of the structures in the wake. The convective velocity is estimated by computing the spatial cross-correlation of a strip of pressure values in the wake between two realizations of the DMD mode. Each realization is done by taking the spatial mode information and prescribing a phase, $P_1 = e^{\varphi_1}\phi_k\left(\vec{x}\right)$ The phase between two modes, $\Delta\varphi = \varphi_2 - \varphi_1$, can be determined from the prescribed phases. The chosen strip in the wake of the turret for St = 1 and M = 0.65 is shown in Figure 18. The convective velocity can be determined using

$$U_C = \frac{dx}{dt}, dt = \frac{1}{f}\frac{\Delta\varphi}{2\pi}$$

$$U_C = dxf\,\frac{2\pi}{\Delta\varphi}$$

Here *dx* is the location of the peak of the cross-correlation between two generated frames, and *dt* is the time delay between the two generated frames. The time delay between two phases of a given mode is a function of the modal frequency, *f* and the prescribed phase delay, $\Delta\varphi$, where one full cycle at the frequency is equivalent to 2π of phase. Thus, by determining the peak location of the cross-correlation function between two frames with a prescribed phase delay and modal frequency, the convective velocity of a mode in a given region can be determined. To improve the accuracy of the peak, the average correlation across various phase delays is computed. The average correlation function for St = 1 at M = 0.65 is shown in Figure 19.

The convective speeds as a function of Strouhal number for both incoming Mach numbers is shown in Figure 20. In the wake, the smaller structures are convecting at 60% of the freestream velocity at M = 0.65. At M = 0.55, the convective velocity in the wake is found to be moving slightly slower, at about 50% of freestream velocity. The exact reason for this difference isn't obvious from this analysis, but it warrants future investigation. For both Mach numbers, this occurs across the range of Strouhal numbers from $0.5 \leq St \leq 2$, meaning that both wakes exhibit similar behavior.

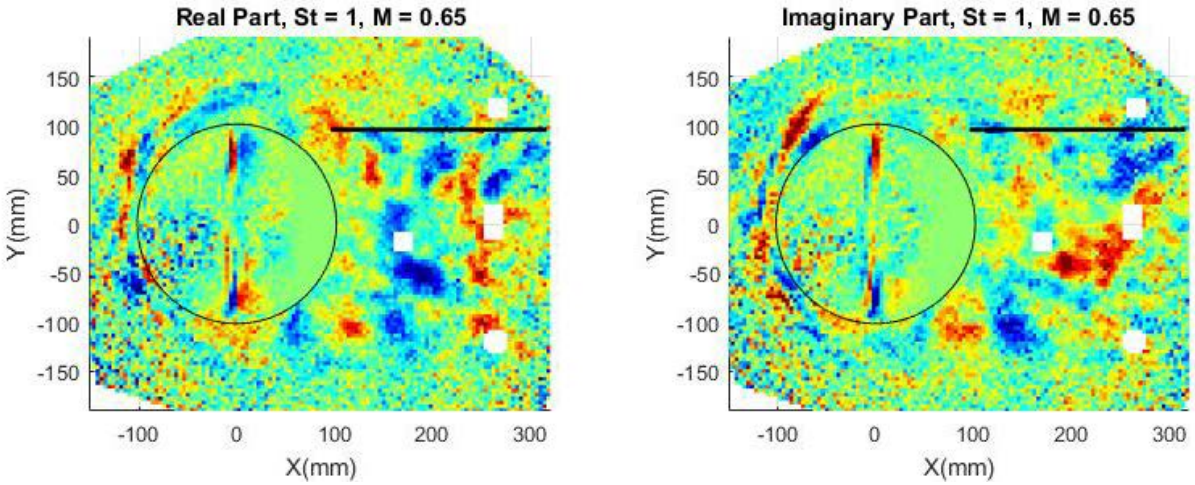

Figure 18: DMD Modes for St = 1, M = 0.65. The black line shows the region over which the correlation is performed.

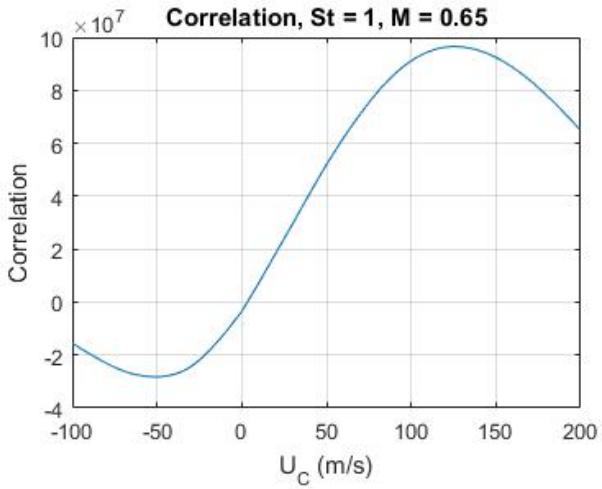

Figure 19: The phase-delay-averaged correlation for St = 1 at M = 0.65.

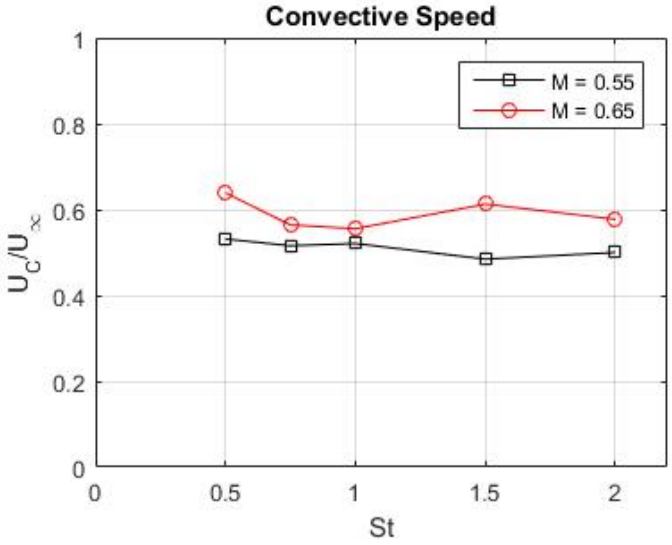

Figure 20: The convective velocity as a function of Strouhal Number at M = 0.65.

V. Conclusions

The unsteady surface pressure field over hemispherical turrets was measured using a fast response Polymer-ceramic/PtTFPPF PSP formulation. Three high speed cameras were used to capture the pressure field at up to 10 kHz. Data were acquired at various Mach numbers to analyze both the subsonic and transonic flow regimes. Though only data for an 8" hemisphere is presented in this paper, data were also acquired for a 10" hemisphere. Unsteady pressure sensors were used to perform in-situ calibration of PSP.

The POD modes of the surface pressure data were computed at M = 0.55 and M = 0.65. Both Mach numbers showed two main wake modes that have been previously proposed [27], a wake "breathing" mode and a wake "shifting" mode. The wake "shifting" mode was dominant for both Mach numbers, but it was represented as a single mode at M = 0.55 and two modes at M = 0.65. The wake "breathing" mode was the second most energetic feature for both Mach numbers. These two dominant wake modes were influenced by the shock over the top of the turret at M = 0.65. The higher order modes represented increasingly small convecting structures in the turret wake. Due to the nature of POD selecting the most energetic features, camera noise corrupted physical modes.

DMD modes were also computed using the surface pressure fields. By analyzing the POD mode temporal coefficient spectra, it is possible to determine the frequencies to investigate using DMD. The lower frequency DMD modes were found to be slow-changing global pressure modes such as the wake "shifting" mode that peaks at St = 0.15-0.2. The "breathing" mode does not have dominant single frequency, so it is not straightforward to isolate it using DMD. The higher frequency DMD modes represent the small, primarily convecting structures in the wake. Knowing the exact frequency of the camera noise, it was also possible to isolate it more effectively using DMD.

The DMD modes were also used to compute the convective velocity in the turret wake. Each mode was correlated with itself at a set phase shift. The average correlation over several phase shifts was computed and the peak in the correlation was used to compute the convective velocity at a given Strouhal number. The structures in the wake was shown to have a relatively constant convective velocity for St > 0.5, with the wake structures moving slightly faster at M = 0.65, relative to the incoming freestream velocity.

Acknowledgments

This work is supported by the Joint Technology Office, Grant number FA9550-13-1-0001 and by AFRL, Contract number FA9451-13-C-0001. The U.S. Government is authorized to reproduce and distribute reprints for governmental purposes notwithstanding any copyright notation thereon.

The authors also would like to thank Dr. Thomas Juliano for his help painting the models and Steve Palluconi from ISSI, Inc. for many useful discussions and recommendations about using PSP.

References

[1] C.H. Snyder, M.E. Franke, M.L. Masquelier, "Wind-Tunnel Tests of an Aircraft Turret Model", Journal of Aircraft,37(3), pp. 368-376, 2000.

[2] R. Sluder, L. Gris, J. Katz, "Aerodynamics of a Generic Optical Turret", Journal of Aircraft, 45(5), pp. 1814-1815,2008.

[3] S. Gordeyev, N. De Lucca, E.J. Jumper, K. Hird, T.J. Juliano, J.W. Gregory, J. Thordahl, and D.J. Wittich, "Comparison of Unsteady Pressure Fields on Turrets with Different Surface Features using Pressure Sensitive Paint", Experiments in Fluids, 55, p. 1661, 2014.

[4] C. Porter, S. Gordeyev, M. Zenk, and E.J. Jumper, "Flight Measurements of the Aero-Optical Environment around a Flat-Windowed Turret", AIAA Journal, 51(6), pp. 1394-1403, 2013.

[5] N. De Lucca, S. Gordeyev, and E.J. Jumper, "In-flight aero-optics of turrets", Journal of Optical Engineering, 52(7), 071405, 2013

[6] J. Morrida, S. Gordeyev and E. Jumper, "Transonic Flow Dynamics Over a Hemisphere in Flight", AIAA Paper 2016-1349, 2016.

[7] E. Mathews, K. Wang, M. Wang and E. Jumper, "LES of an Aero-Optical Turret Flow at High Reynolds Number", AIAA 2016-1461, 2016.

[8] R. Jelic, S. Sherer and R. Greendyke, "Simulation of Various Turret Configurations at Subsonic and Transonic Flight Conditions Using OVERFLOW", Journal of Aircraft, 50, pp. 398-409, 2013.

[9] W.J. Coirier, C. Porter, J. Barber, J. Stutts, M. Whiteley, D. Goorskey, and R. Drye, " Aero-Optical Evaluation of Notional Turrets in Subsonic, Transonic and Supersonic Regimes," AIAA Paper 2014-2355, 2014

[10] P.E. Morgan and M.R. Visbal, "Hybrid Reynolds-Averaged Navier–Stokes/Large-Eddy Simulation Investigating Control of Flow over a Turret," Journal of Aircraft, Vol. 49, No. 6, pp. 1700-1717, 2012.

[11] J. Ladd, A. Mani, and W. Bower, “Validation of Aerodynamic and Optical Computations for the Unsteady Flow Field About a Hemisphere-on-Cylinder Turret,” AIAA Paper 2009-4118, 2009.
[12] S. Gordeyev, and E.J. Jumper, “Fluid Dynamics and Aero-Optics of Turrets", Progress in Aerospace Sciences, 46, pp. 388-400, 2010.
[13] J. Morrida, S. Gordeyev, N. De Lucca, E. Jumper, “Shock-Related Effects on Aero-Optical Environment for Hemisphere-On-Cylinder Turrets at Transonic Speeds, ” Applied Optics, 56(16), pp. 4814-4824, 2017.
[14] D. J. Goorskey, R. Drye and M. R. Whiteley, “Dynamic modal analysis of transonic Airborne Aero-Optics Laboratory conformal window flight-test aero-optics”, Opt. Eng. 52 (7), 071414, 2013.
[15] S. Gordeyev, A. Vorobiev, E. Jumper, S. Gogineni and D.J. Wittich, “Studies of Flow Topology around Hemisphere at Transonic Speeds Using Time-Resolved Oil Flow Visualization”, AIAA Paper 2016-1459, 2016.
[16] B. Vukasinovic, B., Glezer, A., Gordeyev, S., Jumper, E., Kibens, V., “Active Control and Optical Diagnostics of the Flow over a Hemispherical Turret”, AIAA Paper 2008-0598, 2008.
[17] S.J. Beresh, J.F. Henfling, R.W. Spillers, B. O.M. Pruett, “Unsteady Shock Motion in a Transonic Flow over a Wall-Mounted Hemisphere”, AIAA Paper 2013-3201, 2013.
[18] N. De Lucca, S. Gordeyev, E. Jumper, K. Hird, T.J. Juliano, J.W. Gregory, J. Thordahl and D.J. Wittich, “ The Estimation of the Unsteady Aerodynamic Force Applied to a Turret in Flight ”, AIAA Paper 2013-3136, 2013.
[19] G. Berkooz, P. Holmes, and J.L. Lumley, “The proper orthogonal decomposition in the analysis of turbulent flows,” Ann. Rev. Fluid Mech., 25, 539-575, 1993.
[20] P. Holmes, J.L. Lumley, and G. Berkooz, “Turbulence, Coherent Structures, Dynamical Systems and Symmetry”, Cambridge University Press, 1996.
[21] J. Lumley, “Stochastic Tools in Turbulence”, Academic, New York, 1970.
[22] P.J. Schmid. "Dynamic mode decomposition of numerical and experimental data." Journal of Fluid Mechanics 656.1 (2010): 5–28.
[23] K. Taira, S.L. Brunton, S.T.M. Dawson, C.W. Rowley, T. Colonius, B.J. McKeon, O.T. Schmidt, S. Gordeyev, V. Theofilis, and L.S. Ukeiley, "Modal Analysis of Fluid Flows: An Overview," AIAA Journal, 2017, https://doi.org/10.2514/1.J056060
[24] F. Richecoueur, L. Hakim, A. Renaud, L. Zimmer, "DMD Algorithms for Experimental Data Processing in Combustion", Center for Turbulence Research, Summer Proceedings, 2012
[25] Goorskey D., Drye R. and Whitely M., “Dynamic Modal Analysis of Transonic Airborne Aero-Optics Laboratory Conformal Window Flight-Test Aero optics” Optical Engineering 52(7), 071414 (July 2013).
[26] S. Gordeyev, N. De Lucca, J. Morrida, E. Jumper, and D.J. Wittich, “Conditional Studies of the Wake Dynamics Downstream of Hemispherical Turret Using PSP,” AIAA Paper 2018-2048, 2018
[27] N. De Lucca, “Studies of The Pressure Field And Related Beam Jitter For Hemisphere-On-Cylinder Turrets,“ Ph.D. Thesis, University of Notre Dame, 2016.